

# Domination of heliosheath pressure by shock-accelerated pickup ions from observations of neutral atoms

Linghua Wang<sup>1,2</sup>, Robert P. Lin<sup>1,2</sup>, Davin E. Larson<sup>2</sup> & Janet G. Luhmann<sup>2</sup>

The solar wind blows an immense magnetic bubble, the heliosphere, in the local interstellar medium (mostly neutral gas) flowing by the Sun<sup>1</sup>. Recent measurements by Voyager 2 across the termination shock, where the solar wind is slowed to subsonic speeds before entering the heliosheath, found that the shocked solar wind plasma<sup>2</sup> contains only ~20 per cent of the energy released by the termination shock, whereas energetic particles<sup>3</sup> above ~28 keV contain only ~10 per cent; ~70 per cent of the energy is unaccounted for, leading to speculation<sup>2,3</sup> that the unmeasured pickup ions or energetic particles below 28 keV contain the missing energy. Here we report the detection and mapping of heliosheath energetic (~4–20 keV) neutral atoms produced by charge exchange of suprathermal ions with interstellar neutral atoms. The energetic neutral atoms come from a source ~60° wide in longitude straddling the direction of the local interstellar medium. Their energy spectra resemble those of solar wind pickup ions, but with a knee at ~11 keV instead of ~4 keV, indicating that their parent ions are pickup ions energized by the termination shock. These termination-shock-energized pickup ions contain the missing ~70 per cent of the energy dissipated in the termination shock, and they dominate the pressure in the heliosheath.

Energetic neutral atoms (ENAs) are remote tracers of energetic ion populations in distant regions<sup>4</sup>, as they retain the parent ion's velocity in the charge exchange process. In the heliosheath, protons are the dominant ions, hydrogen is the dominant neutral species, and the proton–hydrogen atom cross-section is large, so heliosheath ENAs will be predominantly hydrogen. Furthermore, hydrogen ENAs above ~4 keV have a high probability (>95%) of surviving to the Earth's orbit<sup>4</sup>.

ENAs were detected by the suprathermal electron (STE) sensors<sup>5</sup> of the IMPACT investigation<sup>6</sup> on the STEREO A and B spacecraft from June to October 2007 (Fig. 1). The ENA fluxes peaked near the flow direction of the local interstellar medium (ISM), with a width of ~40–60°. Although these ENAs are observed by different detectors on the two spacecraft at different times over more than ~4 months, the temporal profiles are closely similar (Fig. 2), indicating a distant, steady ENA source such as the heliosheath. The ENA fluxes observed by all the detectors show the same double-peak source structure, extending from ~230° to 290° ecliptic longitude (Fig. 3), with the maximum at ~245° and secondary peak at ~270°, straddling the interstellar gas source direction (254°). The observed longitudinal structure could be due, in part, to latitudinal variations (for example, tilted structures<sup>7</sup>).

The full 360° scan (~March 2007 to March 2008) detected no ENAs (upper limit of  $\sim 2 \times 10^{-3} \text{ cm}^{-2} \text{ s}^{-1} \text{ sr}^{-1} \text{ eV}^{-1}$  at 6.8 keV) from other directions, even though the termination shock should surround the entire heliosphere. For a tear-drop-shaped heliosphere

and the wound-up upstream heliospheric magnetic field, a quasi-perpendicular termination shock (as observed by Voyager 2; ref. 2), which is more efficient than a quasi-parallel shock at accelerating suprathermal ions, would be found near the nose of the heliosphere relative to the interstellar gas flow. Previously reported detections of

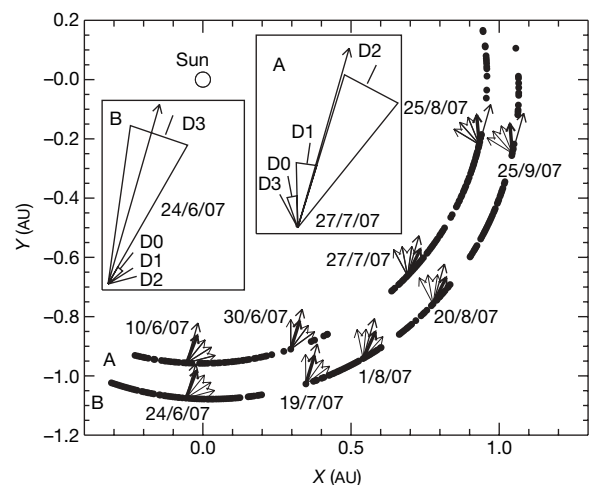


**Figure 1 | The flow direction of energetic neutral atoms in the ecliptic plane.** Main panel, filled circles indicate the location of STEREO A and B when ENAs were detected by the STE<sup>5</sup> sensors of the IMPACT investigation<sup>6</sup>. The gaps occur when the electron background is too high to distinguish ENAs. No ENAs are detected above background at other times in the year (March 2007 to March 2008) when the detectors are pointed in other directions, indicating that the ENA source is limited to ~60° ecliptic longitude around the nose of the heliosphere. For the specified dates, the particle flow direction is indicated by the short thick arrow for the detector observing the maximum ENA flux and by short thin arrows for the other three detectors, while the flow direction of the local ISM is shown by a long arrow. As both spacecraft orbit the Sun, the observed ENA fluxes peak, in turn, in the detector looking roughly towards the incoming local ISM flow. Insets, the anisotropy of 9 keV ENA fluxes observed on 24 June by STEREO B (left inset) and on 27 July by STEREO A (right inset). The latter shows that ENAs are detected by three adjacent detectors, indicating an angular width of ~40–60°. STE utilizes silicon semiconductor detectors with uniquely low thresholds to detect  $\geq 2$  keV electrons, and  $\geq 4$  keV protons/neutral hydrogen. STE-D has four detectors, D0, D1, D2, D3, observing particles coming towards the Sun. Each detector has a field of view covering from 40° S to 40° N in ecliptic latitude by 20° in ecliptic longitude; the fields of view of the four detectors together cover 80° longitude, as shown in the insets. ENAs are identified by their unchanging fluxes and flow direction when the interplanetary magnetic field changes direction (Supplementary Fig. 1), while beams of charged particles will vary with the interplanetary magnetic field.

<sup>1</sup>Physics Department, University of California, Berkeley, California 94720-7300, USA. <sup>2</sup>Space Sciences Laboratory, University of California, Berkeley, California 94720-7450, USA.

$\sim 0.2$  to  $\sim 4\text{--}6$  keV and  $>55$  keV heliosheath ENAs indicate a peak from the tail<sup>8–10</sup> (opposite to the nose), with some evidence for ENAs from our secondary peak<sup>11</sup>.

The measured hydrogen ENA energy spectra fit well to double power laws with a knee at  $\sim 10\text{--}12$  keV (Figs 3 and 4), with low- and high-energy exponents of  $\sim 2\text{--}3$  and  $\sim 4\text{--}7$ , respectively. The hydrogen ENA flux,  $j_{\text{ENA}}$ , is related to the average heliosheath energetic proton flux,  $j_p$ , (assumed isotropic) by:

$$j_{\text{ENA}} = j_p(\sigma_{\text{pH}}n_{\text{H}} + \sigma_{\text{pHe}}n_{\text{He}})L$$

with charge exchange cross-sections of proton–hydrogen and proton–helium respectively  $\sigma_{\text{pH}}$  and  $\sigma_{\text{pHe}}$ , source depth  $L$ , and densities<sup>4,12,13</sup> of neutral He and H respectively  $n_{\text{He}} = 0.015 \text{ cm}^{-3}$  and  $n_{\text{H}} = 9n_{\text{He}}$ . The inferred spectrum of  $j_p$  for the major ENA peak ( $\sim 60\text{--}70^\circ$  in Fig. 3), together with measurements of ions with energies greater than  $\sim 40$  keV (ref. 14) from Voyager 1's nearby crossing of the termination shock at  $\sim 94$  AU (Fig. 4, upper trace) is a double power law with a knee at  $\sim 11$  keV, plus a higher energy power-law tail. This is the same shape as the spectrum of the suprathermal ion population in the outer heliosphere<sup>15</sup>, except there the knee is at  $\sim 4$  keV (due to the maximum speed of twice the solar wind speed for pickup protons). This similarity indicates that the ENA parent heliosheath ions come from the energization of that population by the termination shock<sup>15,16</sup>. The ENA spectrum of the secondary peak is flatter than that of the major peak (Figs 3 and 4), consistent with the flatter spectrum of energetic,  $\geq 28$  keV ions observed by the nearby Voyager 2 crossing<sup>3</sup>.

Voyager 2 (ref. 2) showed that the solar wind slows from  $\sim 310$  to  $\sim 136 \text{ km s}^{-1}$  in crossing the termination shock at  $\sim 84$  AU, thus leading to a downstream energy of  $\sim 1.4 \text{ eV cm}^{-3}$  (Supplementary Table 1). The solar wind plasma is heated only to  $\sim 10^5$  K, so the downstream solar wind flow and thermal energy density (equivalent to the pressure) is only  $\sim 0.26 \text{ eV cm}^{-3}$ . The observed power-law tail<sup>3</sup> of

$\geq 28$  keV ions contains  $\sim 0.1 \text{ eV cm}^{-3}$ , so  $\sim 1 \text{ eV cm}^{-3}$  is missing. The  $\sim 4\text{--}20$  keV heliosheath protons (inferred from the ENAs) near the Voyager 2 termination shock crossing location (Fig. 3) have an energy density of  $\sim 0.1 \text{ eV cm}^{-3}$ , but if these are termination-shock-heated pickup ions, their spectrum should extend down to solar wind energies ( $\lesssim 0.2$  keV); if this is so, then their energy density is  $\sim 1 \text{ eV cm}^{-3}$ , equal to the 'missing' energy, and their number density is  $\sim 1.8 \times 10^{-3} \text{ cm}^{-3}$ ,  $\sim 75\%$  of the solar wind.

Voyager 2 observed the solar wind speed to decrease in three steps, from  $\sim 400 \text{ km s}^{-1}$  starting 0.7 AU upstream, to  $\sim 300 \text{ km s}^{-1}$  at the termination shock<sup>2</sup>, possibly due to the addition of  $\sim 30\%$  to the solar wind density<sup>17</sup> in new pickup ions from ionization of interstellar neutrals by enhanced fluxes of energetic electrons<sup>3</sup> from the termination shock. Pickup ions accumulated previously should be a similar fraction<sup>4</sup>, for a total close to 75%. Thus, most of the energy released by the termination shock is likely to go into heating the pickup protons<sup>15</sup>, and these ions dominate the downstream pressure.

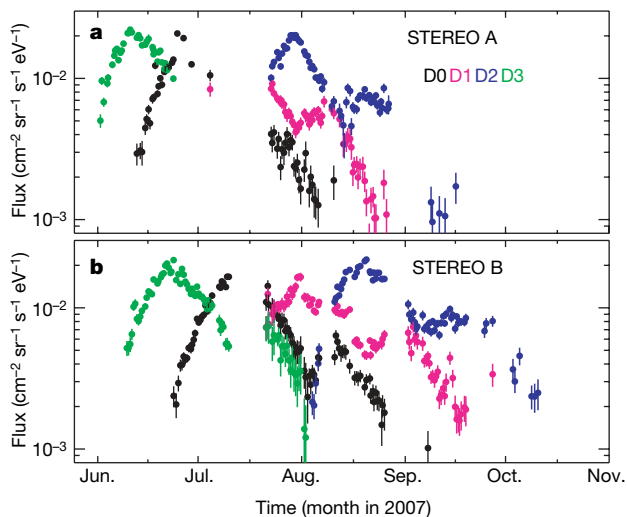


**Figure 2 | The temporal variation of the 6.8 keV hydrogen ENA flux.** Each filled circle indicates an average flux over a 2-h low-background period observed by STE-D (black, D0; pink, D1; blue, D2; green, D3). Each detector's field of view scans a full  $360^\circ$  ecliptic longitude during the year (March 2007 to March 2008). The temporal profile of the ENA flux is similar for all detectors; however, the flux peaks on 23 June in D3, 31 July in D1 and 20 August in D2 for STEREO B (b), while it peaks about 10–20 days earlier for STEREO A (a). No ENAs are detected above background at other times. In addition, the ENA flow is detected by three adjacent detectors during July–August and July–September for STEREO A and STEREO B, respectively, indicating a source region of  $\geq 40\text{--}60^\circ$  width in ecliptic longitude. Error bars, s.e.m. The fluxes below  $\sim 10^{-3} \text{ cm}^{-2} \text{ sr}^{-1} \text{ s}^{-1} \text{ eV}^{-1}$  are not statistically significant.

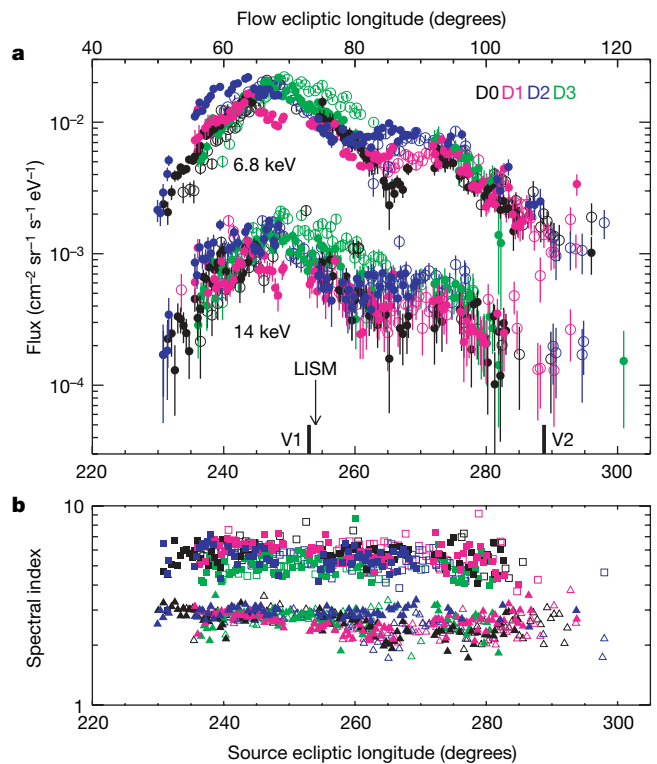


**Figure 3 | The map of the heliosheath source of ENAs versus ecliptic longitude.** Colour (black, pink, blue and green) indicates detectors (D0, D1, D2 and D3, respectively); open (filled) symbols show the data for STEREO A (B). **a**, The intensity of the ENA fluxes ( $\text{cm}^{-2} \text{ sr}^{-1} \text{ s}^{-1} \text{ eV}^{-1}$ ) at  $\sim 6.8$  and 14 keV, plotted versus their source direction in ecliptic longitude (flow direction = source direction minus  $180^\circ$ , indicated at top). The arrow indicates the relative flow direction between the local ISM and Sun. The two short, thick vertical lines indicate the longitudes of the Voyager 1 (V1) and Voyager 2 (V2) crossings of the termination shock. Error bars, s.e.m.; LISM, local ISM. The ENA fluxes observed by different detectors show the same double-peak source structure as a function of ecliptic longitude from  $\sim 230^\circ$  to  $290^\circ$ . No statistically significant ENA enhancement is detected at other ecliptic longitudes. The maximum occurs at  $\sim 240\text{--}250^\circ$ , while the secondary, weaker peak is at  $\sim 270^\circ$ . Each peak is  $\sim 20^\circ$  full-width at half-maximum,  $\sim 30\text{--}40$  AU wide, assuming the source is  $\sim 100$  AU away. The differences between detectors may reflect temporal variations. **b**, The exponent below the  $10\text{--}12$  keV knee (triangles) and above (squares) for the double power-law fit to the ENA spectrum. For the stronger peak, the average power-law exponent is  $\sim 2.8$  below the knee (10.9 keV) and  $\sim 5.6$  above; for the weaker peak it is slightly flatter,  $\sim 2.5$  below the break (10.7 keV) and  $\sim 5.4$  above. This spectral difference may reflect the variability in space rather than in time, as it is seen by different detectors at different times.

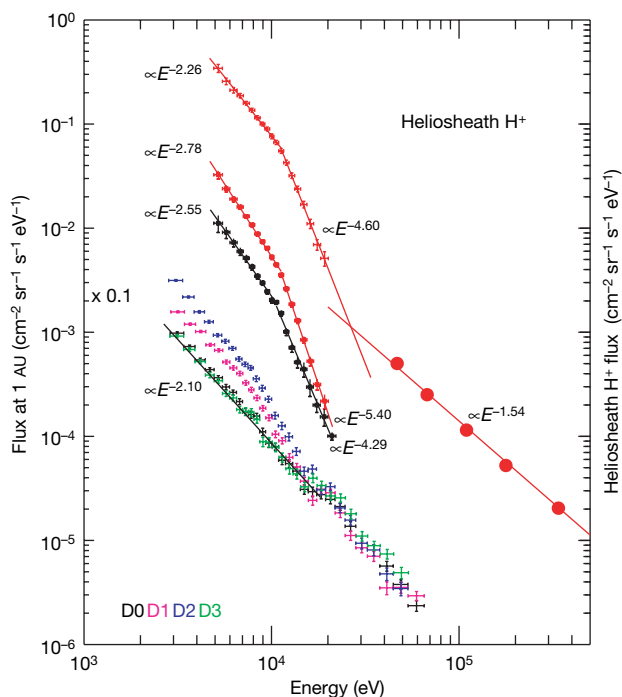


**Figure 4 | Energy spectra of the particles.** Bottom set of curves, STEREO B 9 September 2007 measured fluxes (divided by 10) versus energy (assuming electrons) in detectors D0, D1, D2, D3. D0 and D3 (black and green) measure the isotropic suprathermal electrons in the solar wind, well fitted (black line) by a power law with exponent  $\sim 2.1$ . The flattening around 20 keV is due to leakage from the onboard X-ray calibration source. The enhanced fluxes in the other two directions, D1 and D2 (pink and blue), at energies below  $\sim 15$  keV are due to ENAs. Error bars here and in all curves represent s.e.m. Middle pair of curves, squares show ENA hydrogen spectra (red, maximum; black, secondary peak) at  $\sim 1$  AU. These spectra are obtained by subtracting the electron background and correcting for the energy loss through the detector window (Supplementary Information). They fit to a double power law with exponents of  $\sim 2.8$  and  $2.6$  below the knee ( $\sim 11$  keV) and of  $\sim 5.4$  and  $4.3$  above, for the maximum (from near Voyager 1 crossing) and secondary peak (from near Voyager 2 crossing), respectively. Top curves, red symbols with error bars show the parent suprathermal proton fluxes (assumed isotropic) in the heliosheath, inferred from the ENA measurements at  $\sim 1$  AU for the maximum. They fit to a double power law with exponent of  $2.3$  below the  $11$  keV knee and  $4.6$  above. We assume the distance to the ENA source is  $\sim 100$  AU, and the source is  $40$  AU (equal to its FWHM width) deep. Red filled circles show the Voyager 1 measurements of the *in situ* heliosheath proton fluxes at energies above  $\sim 40$  keV (ref. 14), after its termination shock crossing close to the ENA maximum location. Thus, the combination of these two spectra is representative of the heliosheath ion spectrum.

The ENA fluxes sometimes show significant differences between detectors (Fig. 3: longitude ranges of  $235\text{--}240^\circ$ ,  $245\text{--}248^\circ$ ,  $253\text{--}270^\circ$ ), suggesting variability on a tens-of-days scale, perhaps from solar

wind changes (but probably unrelated to the approximately hour-scale termination shock magnetic field variability<sup>18</sup>).

Received 16 March; accepted 1 May 2008.

1. Axford, W. I. *et al.* in *Solar Wind* (eds Sonett, G. P., Coleman, P. J. Jr & Wilcox, J. M.) 609–660 (Spec. Publ. 308, NASA, Washington DC, 1972).
2. Richardson, J. D., Kasper, J. C., Wang, C., Belcher, J. W. & Lazarus, A. J. Cool heliosheath plasma and deceleration of the upstream solar wind at the termination shock. *Nature* doi:10.1038/nature07024 (this issue).
3. Decker, R. B. *et al.* Mediation of the solar wind termination shock by non-thermal ions. *Nature* doi:10.1038/nature07030 (this issue).
4. Gruntman, M. *et al.* Energetic neutral atom imaging of the heliospheric boundary region. *J. Geophys. Res.* **106**, 15767–15781 (2001).
5. Lin, R. P. *et al.* The STEREO IMPACT Suprathermal Electron (STE) instrument. *Space Sci. Rev.* doi:10.1007/s11214-008-9330-7 (in the press).
6. Luhmann, J. G. *et al.* STEREO IMPACT investigation goals, measurements, and data products overview. *Space Sci. Rev.* doi:10.1007/s11214-007-9170-x (in the press).
7. Heerikhuisen, J. *et al.* The effects of global heliospheric asymmetries on energetic neutral atom sky maps. *Astrophys. J.* **655**, L53–L56 (2007).
8. Hilchenbach, M. *et al.* Detection of 55–80 keV hydrogen atoms of heliospheric origin by CELIAS/HSTOF on SOHO. *Astrophys. J.* **503**, 916–922 (1998).
9. Gallii, A. *et al.* Direct measurements of energetic neutral hydrogen in the interplanetary medium. *Astrophys. J.* **644**, 1317–1325 (2006).
10. Wurz, P. *et al.* in *Physics of the Inner Heliosheath* (eds Heerikhuisen, J., Florinski, V., Zank, G. P. & Pogorelov, N. V.) 269–275 (AIP Conf. Proc. 858, AIP, New York, 2006).
11. Collier, M. R. *et al.* An unexplained  $10\text{--}40^\circ$  shift in the location of some diverse neutral atom data at 1 AU. *Adv. Space Res.* **34**, 166–171 (2004).
12. Witte, M. *et al.* Kinetic parameters of interstellar neutral helium: Final results from the ULYSSES/GAS Instrument. *Adv. Space Res.* **34**, 61–65 (2004).
13. Gloeckler, G. *et al.* Observations of the helium focusing cone with pickup ions. *Astron. Astrophys.* **426**, 845–854 (2004).
14. Decker, R. B. *et al.* in *Physics of the Inner Heliosheath* (eds Heerikhuisen, J., Florinski, V., Zank, G. P. & Pogorelov, N. V.) 73–78 (AIP Conf. Proc. 858, AIP, New York, 2006).
15. Gloeckler, G. & Fisk, L. A. in *Physics of the Inner Heliosheath* (eds Heerikhuisen, J., Florinski, V., Zank, G. P. & Pogorelov, N. V.) 153–158 (AIP Conf. Proc. 858, AIP, New York, 2006).
16. Fisk, L. A. *et al.* Acceleration of low-energy ions at the termination shock of the solar wind. *Astrophys. J.* **644**, 631–637 (2006).
17. Richardson, J. D., Paularena, K. I., Lazarus, A. J. & Belcher, J. W. Evidence for a solar wind slowdown in the outer heliosphere? *Geophys. Res. Lett.* **22**, 1469–1472 (1995).
18. Burlaga, L. F. *et al.* Magnetic fields at the solar wind termination shock. *Nature* doi:10.1038/nature07029 (this issue).

**Supplementary Information** is linked to the online version of the paper at [www.nature.com/nature](http://www.nature.com/nature).

**Acknowledgements** We thank R. Mewaldt for suggestions, G. Gloeckler and E. Roelof for discussions, D. Curtis for instrument development and explanations of calibration data, and the Voyager team for sharing their results before publication. This research was supported in part by the National Aeronautics and Space Administration.

**Author Contributions** L.W. analysed the data and wrote the paper with direction and help from R.P.L. R.P.L. designed the Suprathermal Electron instrument and is the co-investigator in charge. D.E.L. assisted with the experimental work. J.G.L. is the principal investigator of the IMPACT investigation on STEREO that includes STE.

**Author Information** Reprints and permissions information is available at [www.nature.com/reprints](http://www.nature.com/reprints). Correspondence and requests for materials should be addressed to L.W. ([windsound@ssl.berkeley.edu](mailto:windsound@ssl.berkeley.edu)).